Presented at the 18th Annual CMAS Conference, Chapel Hill, NC, October 21-23, 2019

NUMERICAL EVALUATION OF THE IMPACTS OF EMISSION AND METEOROLOGICAL CHARACTERISTICS ON AIR POLLUTION IN THE SETO INLAND SEA REGION, JAPAN

Hikari Shimadera*, Shin Araki, Shota Iida, Tomohito Matsuo and Akira Kondo
Osaka University, Suita, Osaka, Japan

Tatsuya Sakurai
Meisei University, Hino, Tokyo, Japan

Syuichi Itahashi and Hiroshi Hayami
Central Research Institute of Electric Power Industry, Abiko, Chiba, Japan

1. INTRODUCTION

The Seto Inland Sea (SIS) region in the Chugoku-Shikoku (CS) region of Japan is characterized by higher air pollution level compared to the other regions in the country. The SIS region includes SIS with heavy ship traffic volume and its industrialized coastal areas with a number of large point sources (LPSs). In addition, the SIS region is surrounded by mountains in the CS region, which may result in meteorological conditions that suppress atmospheric ventilation. This study evaluates the impacts of local emission and meteorological characteristics on air pollution in the SIS region as well as the surrounding region (the other CS (OCS) region).

2. METHOD

Air quality simulations were conducted with the Community Multiscale Air Quality model (CMAQ) (Byun and Schere, 2006) v5.2.1 in a study period from April 2013 to March 2014 (Japanese fiscal year 2013: JFY2013) with an initial spin-up period of 22-31 March 2013. The study period was selected because the year had a relatively large number of high $PM_{2.5}$ concentration days among recent years. Fig. 1 shows three nested CMAQ domains covering East Asia (D1), Western Japan (D2) and the SIS and OCS regions (D3). The horizontal resolutions and the grid cell numbers were 45 km and 127 × 107 for D1, 15 km and 86 × 66 for D2, and 5 km and 96 × 54 for D3, respectively. There were 30 vertical layers from the surface to 100 hPa with the height of the first layer being approximately 50 m. The SIS and OCS regions in this study were defined as the regions

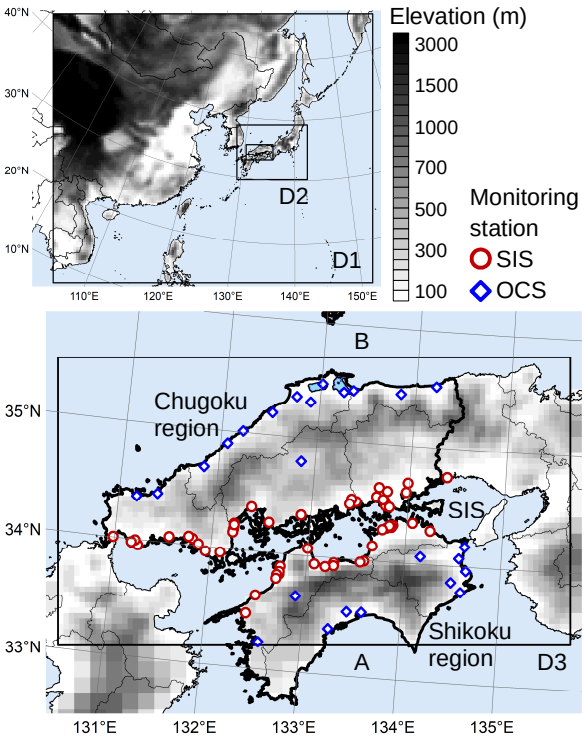

Fig. 1. Modeling domains and location of ambient $PM_{2.5}$ monitoring stations in the SIS and OCS regions in D3.

with distances less than 5 km and more than 20 km from the SIS coastal lines in the CS region, respectively. The model performance was evaluated with observed data at ambient air pollution monitoring stations with observations of $PM_{2.5}$ concentration in the SIS and OCS regions (Fig. 1).

Meteorological fields were produced by the Weather Research and Forecasting model (WRF) (Skamarock and Klemp, 2008) v3.8. The physics options and objective analysis data were the Yonsei University planetary boundary layer (PBL) scheme, the Kain cumulus parameterization for D1 and D2, the WRF single-moment 6-class

*Corresponding author: Hikari Shimadera, Osaka University, 2-1 Yamada-oka, Suita, Osaka 565-0871 Japan; e-mail: shimadera@see.eng.osaka-u.ac.jp

microphysics scheme, the Noah land surface model, the rapid radiative transfer model for the long wave radiation, the Dudhia scheme for the shortwave radiation, the real time, global analysis, high-resolution sea surface temperature (RTG_SST_HR) data by the U.S. National Centers for Environmental Prediction (NCEP), the mesoscale model grid point value (MSM-GPV) data by the Japan Meteorological Agency (JMA) and the final analysis (FNL) data by NCEP. Grid nudging was applied to horizontal wind components, temperature and humidity with nudging coefficients of 1.5×10^{-4} s^{-1} for D1 and D2, and 0.5×10^{-4} s^{-1} for D3 in the entire simulation domain and period.

CMAQ was configured with the Statewide Air Pollution Research Center v2007 (SAPRC07) gas-phase chemistry mechanism and the sixth generation CMAQ aerosol module (AERO6). The hourly WRF results were processed using the Meteorology-Chemistry Interface Processor (MCIP) v4.5 for CMAQ. Boundary concentrations of D1 were derived from the Model for Ozone and Related Chemical Tracers v4 (MOZART-4) (Emmons et al., 2010).

Anthropogenic emissions in Japan were derived from the Japan Auto-Oil Program (JATOP) Emission Inventory-Data Base (JEI-DB) developed by Japan Petroleum Energy Center (JPEC, 2012) for vehicles, an emission inventory developed by the Ocean Policy Research Foundation (OPRF, 2013) for ships, and an emissions inventory called EAGrid2010-JAPAN (Fukui et al., 2014) for the other sectors. Anthropogenic emissions in East Asia except Japan were derived from the Task Force Hemispheric Transport of Air Pollution emission inventory v2.2 (Janssens-Maenhout et al., 2015). Although the study period is JFY2013 and the base year of the above-mentioned inventories is 2010, no year adjustment was applied to the anthropogenic emissions. Daily emissions from open biomass burning were derived from the Fire INventory (FINN) (Wiedinmyer et al., 2011) v1.5 developed by the National Center for Atmospheric Research (NCAR). Biogenic emissions were estimated with the Model of Emissions of Gases and Aerosols from Nature (MEGAN) v2.04 (Guenther et al., 2006). Baseline volcanic SO_2 emissions were derived from the Aerosol Comparisons between Observations and Models (AEROCOM) data (Diehl et al., 2012).

Fig. 2 shows spatial distributions of mean SO_2 and primary $PM_{2.5}$ emissions in D3. Major anthropogenic emission sources are ships and LPSs in D3. The total SO_2 and primary $PM_{2.5}$ emissions in D3 were 192 Gg yr^{-1} with 60 and 124 Gg yr^{-1} from ships and LPSs and 38 Gg yr^{-1} with 12 and 11 Gg yr^{-1} from ships and LPSs, respectively.

In order to evaluate the impacts of local emission and meteorological characteristics on air pollution in the SIS region, the CMAQ simulations were conducted for the following 4 emission cases: the baseline case with the entire emissions described above, two zero-out emission cases for SO_x from ships and from land area (roughly equivalent to LPSs) in D3, a passive tracer (non-reactive and no deposition) case with constant and homogeneous emission in the first layer over D3 area. The contribution of SO_x emissions from in D3 was estimated from the difference between the baseline simulation case and a zero-out emission case. The passive tracer was used as an indicator for ventilation efficiency, i.e., high tracer concentration indicates longer atmospheric retention.

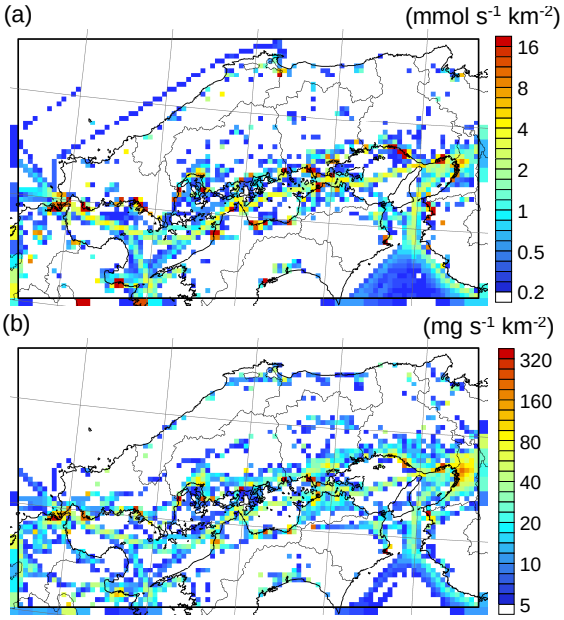

Fig. 2. Spatial distributions of annual mean (a) SO_2 and primary (b) $PM_{2.5}$ emissions in D3.

3. RESULTS AND DISCUSSION

3.1 Model Performance

The CMAQ performance of the baseline simulation was evaluated by comparing observed and simulated SO_2 and $PM_{2.5}$ concentrations at the monitoring stations in D3 (Fig. 1).

Fig. 3 shows time series comparisons of

observed and simulated daily mean SO_2 and $PM_{2.5}$ concentrations averaged for the SIS monitoring stations. The model fairly well simulated day-to-day variations of the concentrations including occurrence of several high concentration peaks in the SIS region. Fig. 4 shows comparisons of observed and simulated differences between the SIS and OCS regions in daily mean SO_2 and $PM_{2.5}$ concentrations averaged for the monitoring stations. The concentrations were generally higher in the SIS region than in the OCS region, and the simulated differences well correlated with the observed differences.

Fig. 5 shows spatial distributions of simulated annual mean SO_2 and $PM_{2.5}$ concentrations in D3. The concentrations were higher over the SIS region, with clearer contrast in SO_2 than in $PM_{2.5}$, indicating the impacts of local emissions. A decreasing trend from west to east in the background concentrations indicates the larger impacts of long-range transport from the Asian Continent on the western Japan.

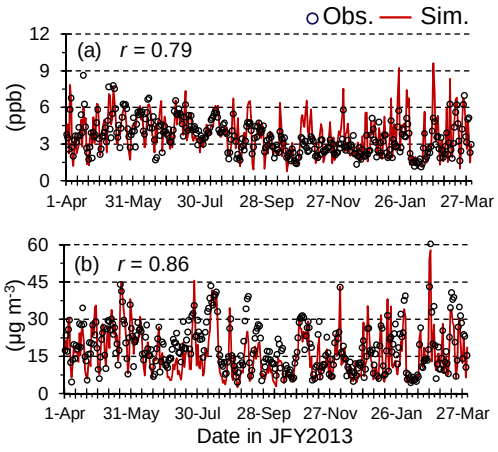

Fig. 3. Time series of observed and simulated daily mean (a) SO_2 and (b) $PM_{2.5}$ concentrations averaged for all the SIS monitoring stations. Values of the Pearson's correlation coefficient are provided.

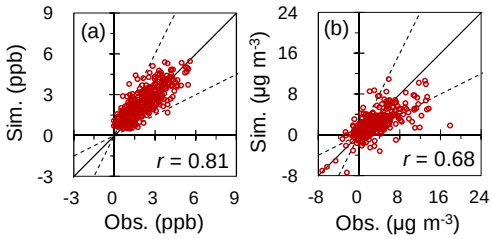

Fig. 4. Scatter plots for observed and simulated differences between the SIS and OCS regions in daily mean (a) SO_2 and (b) $PM_{2.5}$ concentrations averaged for all the monitoring stations. Positive values indicate higher concentrations in the SIS region than in the OCS region. Values of the Pearson's correlation coefficient are provided.

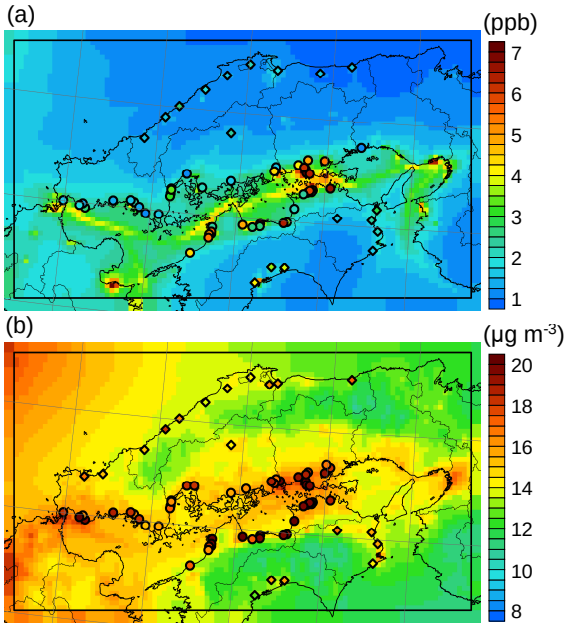

Fig. 5. Horizontal distributions of simulated annual mean (a) SO_2 and (b) $PM_{2.5}$ concentrations in D3 with corresponding observed concentrations at the monitoring stations.

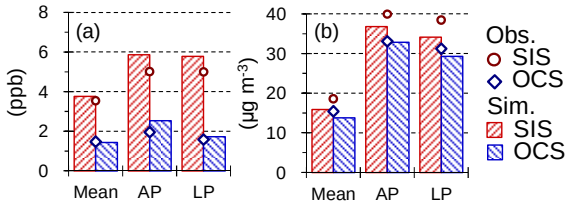

Fig. 6. Observed and simulated mean (a) SO_2 and (b) $PM_{2.5}$ concentrations for all, AP and LP days averaged for the SIS and OCS monitoring stations.

Fig. 6 shows comparisons of mean SO_2 and $PM_{2.5}$ concentrations for all days, air pollution (AP) days and local air pollution (LP) days averaged for the monitoring stations in the SIS and OCS regions. In this study, AP days are defined as days with median values of observed daily mean $PM_{2.5}$ concentrations > 35 μg m^{-3} at the SIS stations (23 days), and LP days are defined as AP days with mean contributions of SO_x emissions in D3 to SO_2 concentrations at the SIS stations > 70% (7 days). Although the model slightly overestimated and underestimated SO_2 and $PM_{2.5}$ concentrations respectively, it well simulated mean differences in the concentrations between not only non-pollution and pollution days but also the SIS and OCS regions. Because the AP days include pollution

days with large impacts of long-range transport, the mean concentrations on the AP days in the OCS region with small local emissions are higher than those on LP days. In addition, the differences between the SIS and OCS regions on the LP days were larger than those on the AP days.

Overall, the results of the performance evaluation indicate that the model successfully captured the characteristics of air pollution in the SIS region.

3.2 Impacts of Local SO_x Emission

The impacts of local SO_x emissions from ships and land areas were estimated from the difference between the baseline simulation case and the zero-out emission cases for SO_x emissions from ships and land areas in D3, respectively.

Fig. 7 shows spatial distributions of estimated annual mean contribution rates of total SO_x emissions in D3 to SO_2 and $PM_{2.5}$ concentrations. Fig. 8 shows estimated mean contributions of SO_x emissions from ships and land areas in D3 to SO_2 and $PM_{2.5}$ concentrations for all, AP and LP days averaged for the SIS and OCS monitoring stations. For the absolute contribution, the mean contributions of SO_x emissions in D3 to SO_2 and $PM_{2.5}$ concentrations in the SIS region were 5.1 and 2.8 times for annual mean, 5.3 and 2.7 times for the AP days, and 6.0 and 2.6 times for the LP days higher than those in the OCS region,

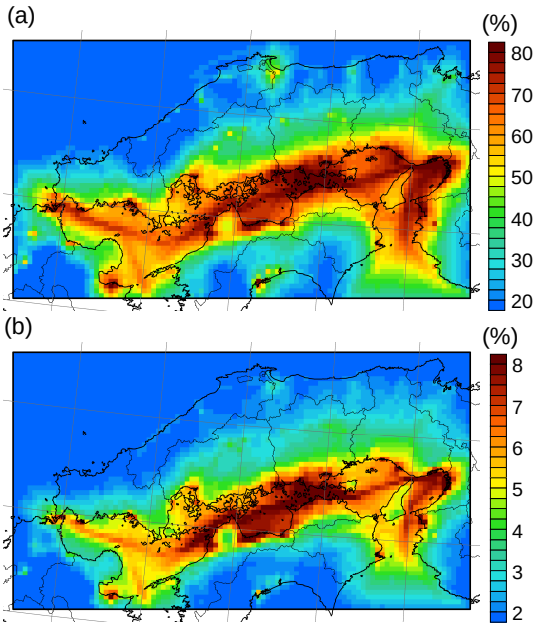

Fig. 7. Horizontal distributions of estimated annual mean contribution rates of total SO_x emissions in D3 to (a) SO_2 and (b) $PM_{2.5}$ concentrations.

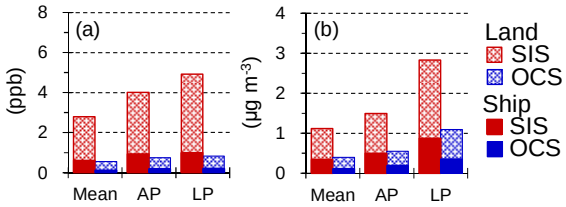

Fig. 8. Simulated mean contributions of SO_x emissions from ships and land areas in D3 to (a) SO_2 and (b) $PM_{2.5}$ concentrations for all, AP and LP days averaged for the SIS and OCS monitoring stations.

respectively. For the relative contribution, the annual mean contribution rates of SO_x emissions in D3 to SO_2 and $PM_{2.5}$ concentrations were 75.2% (16.6%: ships, 58.6%: land areas) and 7.1% (2.2%: ships, 4.9%: land areas) at the SIS stations, and 37.7% (8.6%: ships, 29.1%: land areas) and 2.9% (0.9%: ships, 2.0%: land areas) at the OCS stations, respectively. The mean contribution rates to SO_2 and $PM_{2.5}$ concentrations were 69.2% (16.1%: ships, 53.2%: land areas) and 4.0% (1.4%: ships, 2.7%: land areas) on the AP days and 86.6% (17.6%: ships, 69.0%: land areas) and 8.2% (2.5%: ships, 5.7%: land areas) on the LP days at the SIS stations, respectively.

Both the absolute and relative contributions of local SO_x emissions are much larger in the SIS region than in the OCS region. In addition, both the absolute and relative contributions were the largest on the LP days at the SIS stations. These results indicate that the emission characteristics in the SIS region, heavy ship traffic volume and a large number of LPSs, obviously contribute to the occurrence of LP in the region.

3.3 Impacts of Local Meteorology

The contribution of local emissions shown in Figs. 7 and 8 reflects the impacts of both local emission and meteorological characteristics. The passive tracer was utilized in order to evaluate the impacts of ventilation efficiency as the local

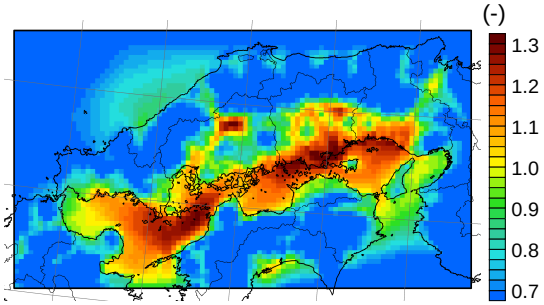

Fig. 9. Horizontal distribution of simulated annual mean tracer concentration in D3.

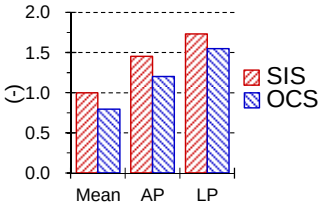

Fig. 10. Simulated mean tracer concentrations for all, AP and LP days averaged for the SIS and OCS monitoring stations.

meteorological characteristics on air pollution in the SIS region. The tracer concentration was normalized by annual mean concentration averaged for the SIS monitoring stations.

Fig. 9 shows spatial distributions of simulated annual mean tracer concentration in D3. The tracer concentration was higher in basin areas and lower in mountainous areas, validating it as an effective indicator for regional characteristics of ventilation efficiency. The tracer concentration in the SIS region was comparable to that in the basin areas, which indicates that the local meteorological characteristics suppress atmospheric ventilation in the SIS region.

Fig. 10 shows simulated mean concentrations for all, AP and LP days averaged for the SIS and OCS monitoring stations. The tracer concentration was the highest on the LP days as a result of low ventilation efficiency. The tracer concentration was consistently higher in the SIS region than in the OCS region, with the mean value in the SIS region being higher by 26%, 21% and 12% than that in the OCS region for annual mean, the AP and LP days, respectively.

In order to further investigate the impacts of the local meteorological characteristics on air pollution in the SIS region, Figs. 11 and 12 respectively show horizontal and vertical

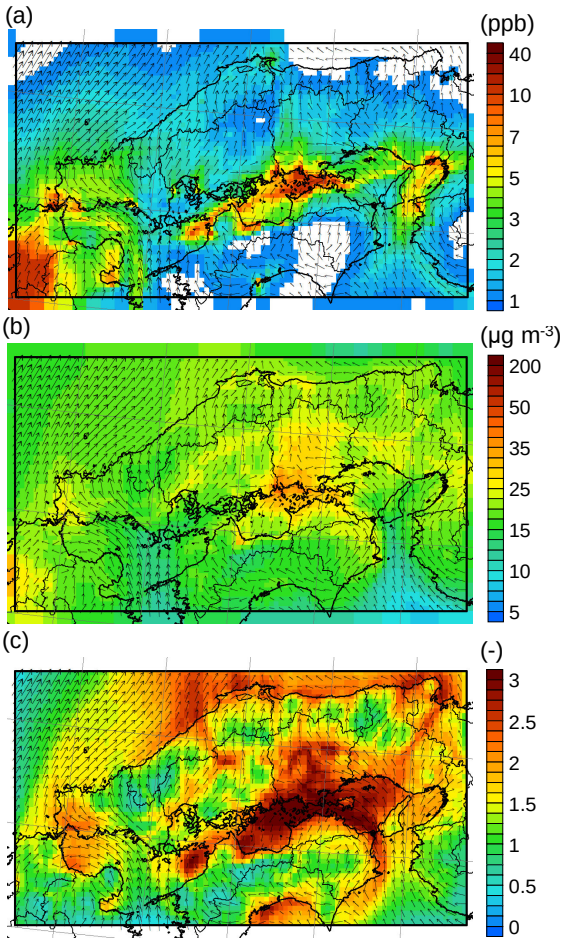

Fig. 11. Horizontal distributions of simulated mean (a) SO_2, (b) $PM_{2.5}$ and (c) tracer concentrations in D3 on September 13, 2013 as a typical LP day.

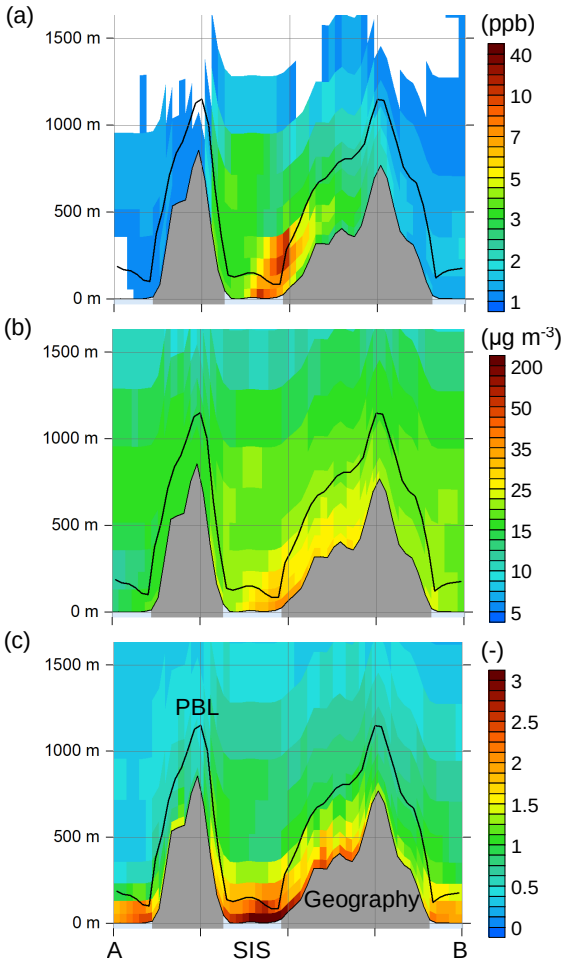

Fig. 12. Vertical cross sections of simulated mean (a) SO_2, (b) $PM_{2.5}$ and (c) tracer concentrations along A-B in Fig. 1 on September 13, 2013 as a typical LP day.

distributions of simulated mean SO_2, $PM_{2.5}$ and tracer concentrations on September 13, 2013 as a typical LP day. Local high concentrations were distributed in the SIS region. In the region, the PBL height was lower than the surrounding mountains, which favored the accumulation of locally emitted pollutants.

These results indicate that the meteorological characteristics in the SIS region contribute to the enhancement of local accumulation of air pollutants in the region.

4. SUMMARY

This study applied CMAQ v5.2.1 to the SIS region in JFY2013 in order to assess the impacts of local emission and meteorological characteristics on air pollution. The model successfully simulated higher SO_2 and $PM_{2.5}$ concentration levels in the SIS region than those in the surrounding regions. The impacts of local emission sources on air pollution were estimated with brute force zero-out runs for SO_x emissions from ships and large point sources. The annual mean contributions of local SO_x emissions to SO_2 and $PM_{2.5}$ concentrations in the SIS region were about 5 and 3 times higher than those in the surrounding regions, respectively. The impacts of local meteorological characteristic on atmospheric ventilation were evaluated with a run with constant passive tracer emission. The annual mean tracer concentration in the SIS region was about 1.3 times higher than that in the surrounding regions, indicating a lower ventilation efficiency in the SIS region. These results show that the local emission and meteorological characteristics mainly and partly contribute to higher air pollution level in the SIS region, respectively.

5. ACKNOWLEDGEMENTS

This research was supported by the Environment Research and Technology Development Fund (5-1802) of the Environmental Restoration and Conservation Agency.

6. REFERENCES

Byun, D., Schere, K. L., 2006: Review of the governing equations, computational algorithms, and other components of the models-3 community multiscale air quality (CMAQ) modeling system. *Appl. Mech. Rev.*, **59**, 51–76.

Diehl, T., Heil, A., Chin, M., Pan, X., Streets, D., Schultz, M., Kinne, S., 2012: Anthropogenic, biomass burning, and volcanic emissions of black carbon, organic carbon, and SO_2 from 1980 to 2010 for hindcast model experiments. *Atmos. Chem. Phys. Discuss.*, **12**, 24895–24954.

Emmons, L. K., Walters, S., Hess, P. G., Lamarque, J.-F., Pfister, G. G., Fillmore, D., Kloster, S., 2010: Description and evaluation of the Model for Ozone and Related chemical Tracers, version 4 (MOZART-4). *Geosci. Model Dev.*, **3**, 43–67.

Fukui, T., Kokuryo, K., Baba, T., Kannari, A., 2014: Updating EAGrid2000-Japan emissions inventory based on the recent emission trends. *J. Japan Soc. Atmos. Environ.*, **49**, 117–125. (in Japanese)

Guenther, A., Karl, T., Harley, P., Wiedinmyer, C., Palmer, P. I., Geron, C., 2006: Estimates of global terrestrial isoprene emissions using MEGAN (Model of Emissions of Gases and Aerosols from Nature). *Atmos. Chem. Phys.* **6**, 3181–3210.

Janssens-Maenhout, G., Crippa, M., Guizzardi, D., Dentener, F., Muntean, M., Pouliot, G., Li, M., 2015. HTAP-v2.2: A mosaic of regional and global emission grid maps for 2008 and 2010 to study hemispheric transport of air pollution. *Atmos. Chem. Phys.*, **15**, 11411–11432.

JPEC. 2012: Technical report of the Japan Auto-Oil Program: emission inventory of road transport in Japan. Tech. Rep. JPEC-2011AQ-02-06 (in Japanese).

OPRF, 2013: Report on the Project for Estimating the Impact of Designation of Emission Control Area on Improvements in Air Quality. Rep. ISBN978-4-88404-282-0, Minato-ku, Tokyo, Japan. (in Japanese)

Skamarock, W. C., Klemp, J. B., 2008: A time-split nonhydrostatic atmospheric model for weather research and forecasting applications. *J. Comput. Phys.*, **227**, 3465–3485.

Wiedinmyer, C., Akagi, S. K., Yokelson, R. J., Emmons, L. K., Al-Saadi, J. A., Orlando, J. J., Soja, A. J., 2011: The Fire INventory from NCAR (FINN): a high resolution global model to estimate the emissions from open burning. *Geosci. Model Dev.*, **4**, 625–641.